Unusual Behavior of the Ferroelectric Polarization in $PbTiO_3/SrTiO_3$ Superlattices

M. Dawber,[1] C. Lichtensteiger,[1] M. Cantoni,[2] M. Veithen,[3] P. Ghosez,[3] K. Johnston,[4] K. M. Rabe,[4] and J.-M. Triscone[1]

[1]*DPMC, University of Geneva, 24 Quai E.-Ansermet 1211 Geneva 4, Switzerland**

[2]*CIME, EPFL, CH-1015 Lausanne, Switzerland*

[3]*Institut de Physique, Université de Liège, Bâtiment B5 Allée du 6 Août, 17 B-4000 Sart Tilman, Belgium*

[4]*Department of Physics and Astronomy, Rutgers University, 136 Frelinghuysen Rd, Piscataway, New Jersey 08854-8019, USA*

(Received 17 June 2005; revised manuscript received 29 July 2005; published 17 October 2005)

Artificial $PbTiO_3/SrTiO_3$ superlattices were constructed using off-axis rf magnetron sputtering. X-ray diffraction and piezoelectric atomic force microscopy were used to study the evolution of the ferroelectric polarization as the ratio of $PbTiO_3$ to $SrTiO_3$ was changed. For $PbTiO_3$ layer thicknesses larger than the 3-unit cell $SrTiO_3$ thickness used in the structure, the polarization is found to be reduced as the $PbTiO_3$ thickness is decreased. This observation confirms the primary role of the depolarization field in the polarization reduction in thin films. For the samples with ratios of $PbTiO_3$ to $SrTiO_3$ of less than one, a surprising recovery of ferroelectricity that cannot be explained by electrostatic considerations was observed.

DOI: 10.1103/PhysRevLett.95.177601 PACS numbers: 77.80.−e, 31.15.Ar, 68.65.Cd, 77.84.Dy

The construction of artificial ferroelectric oxide superlattices with fine periodicity presents exciting possibilities for the development of new materials with extraordinary properties and furthermore is an ideal probe of the fundamental physics of ferroelectric materials.

The most studied system at present is $BaTiO_3/SrTiO_3$ [1–8]. Other combinations that have been studied include $KNbO_3/KTaO_3$ [9–12], $PbTiO_3/SrTiO_3$ [13], $PbTiO_3/BaTiO_3$ [14], $PbTiO_3/PbZrO_3$ [15], and, most recently, high quality tricolor superlattices of $SrTiO_3/BaTiO_3/CaTiO_3$ [16]. In $BaTiO_3/SrTiO_3$, first principles studies [5] suggest that both the $SrTiO_3$ and $BaTiO_3$ layers are polarized such that the polarization is approximately uniform throughout the superlattice. The driving force behind this is the large electrostatic energy penalty for a buildup of charge at the interface caused by discontinuous polarization in the normal direction. Similarly, the electrostatic energy cost of a depolarization field in a ferroelectric thin film with realistic electrodes forces either a decrease in the ferroelectric polarization with reduced thickness [17–20] or, under certain conditions, the formation of domains [21,22]. In this letter we use $PbTiO_3/SrTiO_3$ superlattices to probe the effect of a reduced ferroelectric thickness in a dielectric environment.

The superlattices of $PbTiO_3/SrTiO_3$ were prepared on conducting 0.5% Nb doped (001) $SrTiO_3$ substrates using off-axis rf magnetron sputtering with conditions similar to those used for growing high quality epitaxial c-axis $PbTiO_3$ thin films [20]. For all the samples discussed in this Letter, the $SrTiO_3$ thickness was fixed at three unit cells (about 12 Å). At room temperature the in-plane lattice parameters of tetragonal ferroelectric $PbTiO_3$ ($a = 3.904$ Å, $c = 4.152$ Å) and cubic dielectric $SrTiO_3$ (3.905 Å) are an excellent match [23]. $PbTiO_3$ generally is straightforward to grow coherently on $SrTiO_3$ substrates, and strain interactions are dominated by the constraint imposed by the substrate. The growth temperature for the superlattices was 460 °C (at this temperature $c_{PTO} = 4.02$ Å, $a_{PTO} = 3.935$ Å, $a_{STO} = 3.925$ Å). Investigation by transmission electron microscopy (TEM) revealed excellent quality in superlattices with layers of $SrTiO_3$ thinner than 5 unit cells, though beyond this thickness the quality of the $SrTiO_3$ layers deteriorated with thickness, presumably because of the low temperature. On the other hand, samples processed with higher temperatures were of lower quality, probably because of lead losses from the $PbTiO_3$. The low temperature growth used is thus optimal for making superlattices with very thin $SrTiO_3$ layers, but without limitation on the thickness of $PbTiO_3$.

In the principal series of interest we grew superlattices consisting of 20 $PbTiO_3/SrTiO_3$ bilayers in which the $SrTiO_3$ layer thickness was maintained at 3 unit cells while the $PbTiO_3$ layer thickness n was varied from 54 unit cells down to just one unit cell (denoted $n/3$). The first layer deposited was $PbTiO_3$. The layer thicknesses were calculated from the growth rate determined from x-ray measurements on the whole series of samples.

Cross-sectional TEM investigations were performed on several samples and reveal the coherent growth and artificial layering of the samples. Figure 1 shows a summary of the results obtained on a 3/3 sample. The bright field image, Fig. 1(a), shows the layering throughout the sample. The perfect crystalline structure and coherent growth are demonstrated by the high resolution TEM (HRTEM) image Fig. 1(b), while the periodicity of the superlattice is demonstrated by the superlattice reflections in the diffraction image Fig. 1(c) (arrows).

Further structural characterization was performed using standard θ-2θ x-ray diffraction. Figure 2 shows the θ-2θ scan for a superlattice in which the $PbTiO_3$ layers are 9 unit cells thick and the $SrTiO_3$ layers are 3 unit cells thick (9/3). The periodicity of the superlattice is therefore 12 perovskite unit cells and 12 reflections from $2\theta = 0$ to the angle corresponding to the 001 peak of the average perov-

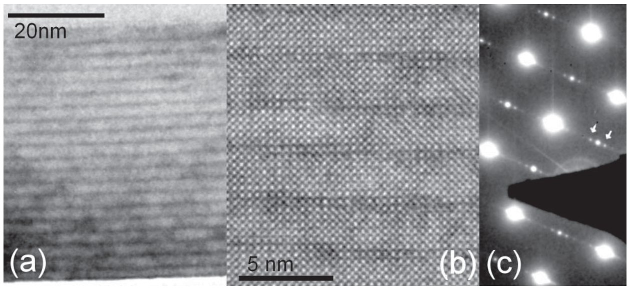

FIG. 1. Cross-sectional TEM images of a 20 bilayer $PbTiO_3/SrTiO_3$ 3/3 sample. (a) Bright field image clearly shows the intended layering of the structure. (b) HRTEM shows the perfect crystalline structure of the material. (c) Diffraction image demonstrating superlattice periodicity.

skite unit cell lattice parameter (at $2\theta \approx 22°$) are expected, most of which are observable in the scan. In between the main superlattice peaks, the presence of 18 finite size effect peaks, clearly visible in the inset of Fig. 2, is due to the finite total thickness of the sample which is 20 times the superlattice periodicity.

Because of the large strain-polarization coupling in $PbTiO_3$ [24], a change in polarization results in a change in material tetragonality [20]. We take advantage of this to follow the evolution of the polarization in the superlattice by following the evolution of the average c axis lattice parameter, $\bar{c}$, as the $PbTiO_3$ layer thickness is varied. If the wavelength of the superlattice is $n\bar{c}$ then the nth (or $2n$th, $3n$th, etc.) peak in a θ-2θ scan will always correspond to $\bar{c}$ irrespective of the value of n allowing the average c axis lattice parameter of the superlattice to be determined [25]. Intuitively, one expects as the thickness of the $PbTiO_3$ layers relative to the $SrTiO_3$ layers is reduced, a decrease of the ferroelectric polarization which should result in a concomitant decrease of the average lattice parameter. The measured average c axis lattice parameters as a function of the thickness of the $PbTiO_3$ layer thickness are shown in Fig. 3. For comparison, we also show the average c axis lattice parameters obtained by fixing c of $SrTiO_3$ at its paraelectric cubic value 3.905 Å and taking c of $PbTiO_3$ in two limiting cases: first, at the value 4.022 Å corresponding to a hypothetical paraelectric tetragonal structure coherent with the substrate (solid line) [20] and then at the fully polarized bulk value 4.152 Å (dashed line). As can be seen in Fig. 3, superlattices with thick $PbTiO_3$ layers have "large" average lattice parameters clearly suggesting a ferroelectric polarization. On reduction of the layer thickness the average lattice parameter decreases and approaches the solid line. However, surprisingly, after reaching this line superlattices with very small $PbTiO_3$ layer thicknesses display larger average lattice parameters which indicate a recovery of ferroelectricity.

This behavior was confirmed using atomic force microscopy (AFM) which allows the ferroelectric domain structure to be modified and detected on a local scale [26]. Applying a voltage between the metallic tip of the AFM and the metallic substrate, stripes were "written" (poled) using alternatively positive and negative voltages. Piezoelectric atomic force microscopy (PFM) was then used to detect the domain structure. PFM images are shown in the insets of Fig. 3 for different superlattices, the contrast revealing domains with up and down polarization. As can be seen, the 1/3, 2/3, and 13/3 samples reveal a clear domain structure and are indeed ferroelectric whereas no significant contrast could be obtained in the 3/3 superlattice, confirming the behavior suggested by the x-ray analysis. The written domains for all samples in which domains could be written were confirmed to be stable for a number of days. All domains written into the down direction have the same piezoelectric response as the existing background, implying that before writing the entire sample is uniformly poled in the down direction, demonstrating that none of the samples formed a polydomain state.

To understand the observed behavior, a simple electrostatic model similar to the one proposed by Junquera and Ghosez [18] has been developed. The total energy per unit cell area E of an n_p/n_s superlattice is written as

$$E(P_p^0, P_s^0) = n_p U_p(P_p^0) + n_s U_s(P_s^0) + E_{\mathrm{elec}}(P_p^0, P_s^0), \quad (1)$$

where U_p and U_s are the total energies per 5-atom unit cell

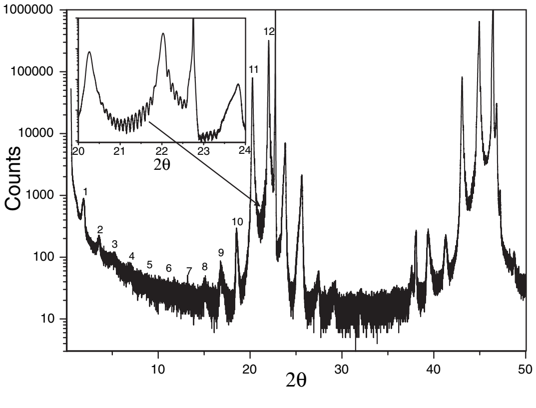

FIG. 2. θ-2θ x-ray diffractogram for a 20 bilayer $PbTiO_3/SrTiO_3$ 9/3 superlattice.

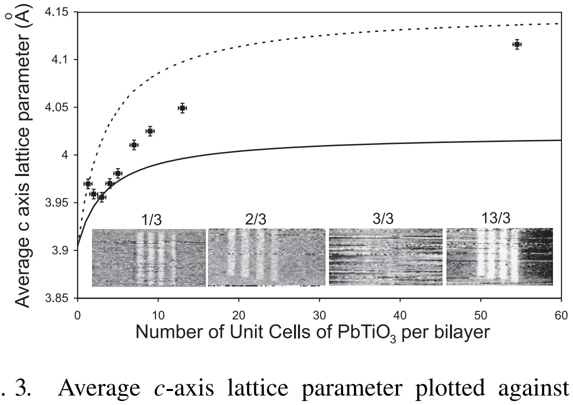

FIG. 3. Average c-axis lattice parameter plotted against the number of unit cells of lead titanate per bilayer showing the suppression and recovery of ferroelectricity. Complementary PFM images are shown as insets.

of bulk $PbTiO_3$ and $SrTiO_3$ in zero field as a function of their polarization P_p^0 and P_s^0 (assumed to be homogeneous in each layer) and $E_{\rm elec}$ is the macroscopic electrostatic energy resulting from the presence of nonvanishing electric fields in the layers when P_p^0 and P_s^0 differ.

The electrostatic energy of a given layer, of thickness l_p or l_s, in the presence of a finite electric field $\mathcal{E}$, to leading order in the field, is $E_{\rm elec} = -l\mathcal{E} \cdot P^0$. In the superlattice, the electric fields $\mathcal{E}_p$ and $\mathcal{E}_s$ are determined by P_p^0 and P_s^0 through the condition of continuity of the normal component of the electric displacement field at the interfaces:

$$P_p^0 + \varepsilon_0 \mathcal{E}_p = P_s^0 + \varepsilon_0 \mathcal{E}_s. \tag{2}$$

For a system under short-circuit boundary conditions, the potential drop along the structure must vanish and

$$l_p \mathcal{E}_p = -l_s \mathcal{E}_s. \tag{3}$$

Combining the last two conditions and summing the electrostatic energies of the $PbTiO_3$ and $SrTiO_3$ layers gives

$$E_{\rm elec}(P_p^0, P_s^0) = \frac{l_p l_s}{\varepsilon_0 (l_p + l_s)} (P_s^0 - P_p^0)^2. \tag{4}$$

The total energies $U_p(P_p^0)$ and $U_s(P_s^0)$ have been obtained from density functional theory (DFT) calculations on bulk compounds using the ABINIT package [27]. The calculations were performed within the local density approximation (LDA) using extended norm conserving pseudopotentials [28] with the Pb ($5d, 6s, 6p$), Sr ($4s, 4p, 5s$), Ti ($3s, 3p, 3d, 4s$), and O ($2s, 2p$) treated as valence states. Convergence was reached for a 1225 eV (45 Ha) cutoff and a $6 \times 6 \times 6$ mesh of special k points. We obtain computed lattice constants for cubic paraelectric $SrTiO_3$ ($a = 3.846$ Å) and for tetragonal ferroelectric $PbTiO_3$ ($a = 3.864$ Å, $c = 3.975$ Å), with a polarization of $0.69\ C/m^2$. Both materials lattice parameters are underestimated relative to the experimental values as is typical for the LDA. For each compound, $U(P^0)$ and $c(P^0)$ were obtained [29] following the formalism of Ref. [30] by relaxing the atomic positions and the lattice parameter c at fixed polarization $P^0 \hat{z}$ in the space group $P4mm$, constraining the in-plane lattice parameter a to 3.846 Å. For bulk $PbTiO_3$ constrained in plane to 3.846 Å the c axis lattice parameter was found to be 4.009 Å with a polarization of $0.73\ C/m^2$. For any choice of n_p and n_s, minimization of Eq. (1) gives equilibrium values for P_p^0 and P_s^0, and thus also for c_p and c_s.

To see whether the model correctly describes the behavior as the thickness of the $PbTiO_3$ layers decreases to the atomic scale, we performed full DFT-LDA calculations of the structure and polarization of $PbTiO_3/SrTiO_3$ superlattices for $n_s = 3$ and $n_p = 1, \ldots 7$ with the Vienna *ab initio* simulations package (VASP) [31], using projector augmented wave (PAW) potentials [32,33] with the same valence configurations as in the ABINIT calculation. Convergence was reached for a 600 eV (22 Ha) cutoff and a $6 \times 6 \times 2$ mesh of special k points. The computed lattice constants are for $SrTiO_3$, $a = 3.86$ Å, and for tetragonal ferroelectric $PbTiO_3$, $a = 3.86$ Å, and $c = 4.047$ Å, with a polarization of $0.75\ C/m^2$ [34]. For the superlattices, the atomic positions and lattice parameter c were fully relaxed in the space group $P4mm$, constraining the in-plane lattice parameter a to 3.86 Å. Polarizations were calculated using the modern theory of polarization [35] as implemented in VASP.

Figure 4(a) shows the evolution of the polarization as a function of $\frac{n_p}{n_s}$ for $n_s = 3$. According both to the model and to the first principles local polarizations (not shown), the difference between the polarizations in the two layers is quite small, highlighting the large electrostatic energy cost of having different polarizations in the layers. As the ratio n_p/n_s increases, the polarization of the superlattice asymptotically approaches the constrained bulk $PbTiO_3$ value, though rather slowly due to the large energy cost of maintaining a high polarization in $SrTiO_3$. The figure inset shows the corresponding increase in the tetragonality (c/a) of the two layers, with the high polarization-strain coupling in the $SrTiO_3$ layer (higher even than for the $PbTiO_3$ layer [29]) being evident. Both the model and the first principles calculations show a monotonic decrease of the polarization as the $PbTiO_3$ volume fraction is reduced, due to the increase in the relative energy cost of the polarization in the $SrTiO_3$ layers. While the polarization vs thickness curve for the model is shifted to lower polar-

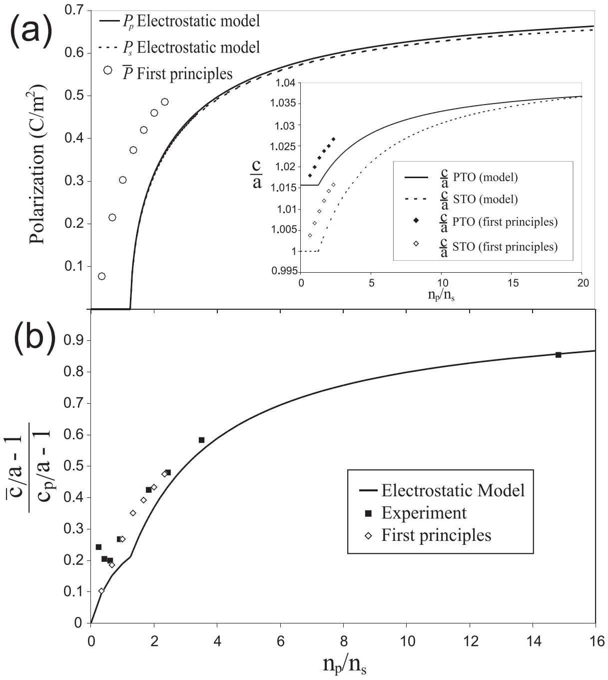

FIG. 4. (a) Polarization in each layer from the electrostatic model (dotted and solid lines) and the average polarization from first principles calculations (open circles). Inset shows tetragonality in each material calculated from both methods. (b) Comparison of experiment and both theoretical approaches.

izations relative to the first principles results, the model works overall very well, considering the simplifying assumptions and lack of any adjustable parameters.

In Fig. 4(b) we compare results from the first principles calculations (open circles), the electrostatic model (solid line) and experiment (solid squares), by plotting the fractional change in the superlattice tetragonality $\frac{\bar{c}}{a} - 1$ relative to the tetragonality of bulk $PbTiO_3$ with the in-plane lattice parameter constrained to the $SrTiO_3$ substrate [34]. Good agreement between both theoretical approaches and experiment is seen for samples that are predominantly $PbTiO_3$. It should be noted that both theoretical calculations are at zero temperature, while the experiments are conducted at room temperature. Specifically this means that samples predicted from first principles to be ferroelectric with a small polarization at zero temperature might be expected to be paraelectric in our room temperature experiment, as is observed in the case of the 3/3 sample. The fact that unexpected recovery of the ferroelectric polarization in the experimental 1/3 and 2/3 superlattices is observed in neither the electrostatic model, nor the first principles calculations, suggests that it is related to aspects not accounted for in our theoretical approaches, for example, the precise nature of the substrate-superlattice interface, some degree of intermixing at the superlattice interfaces, or the possible formation of a new entropically stabilized $PbTiO_3$ phase similar to that formed under negative hydrostatic pressure in the first principles studies of Tinte *et al.* [36].

This work was supported by the Swiss National Science Foundation through the National Center of Competence in Research “Materials with Novel Electronic Properties-MaNEP,” the VolkswagenStiftung (project “Nano-sized ferroelectric hybrids,” I80 899), FNRS-Belgium (Grant No. 2.4562.03), the European NoE FAME and ESF (THIOX), and DOE Grant No. DE-FG02-01ER45937.

---

*Electronic address: matthew.dawber@physics.unige.ch

[1] H. Tabata, H. Tanaka, and T. Kawai, Appl. Phys. Lett. **65**, 1970 (1994).
[2] Y. Ishibashi, N. Ohashi, and T. Tsurumi, Jpn. J. Appl. Phys. **39**, 186 (2000).
[3] O.Nakagawara, T.Shimuta, and T. Makino, Appl. Phys. Lett. **77**, 3257 (2000).
[4] T. Shimuta, O. Nakagawara, and T. Makino, J. Appl. Phys. **91**, 2290 (2002).
[5] J.B. Neaton and K.M. Rabe, Appl. Phys. Lett. **82**, 1586 (2003).
[6] K. Johnston *et al.*, Phys. Rev. B **71**, 100103(R) (2005).
[7] A.Q. Jiang *et al.*, J. Appl. Phys. **93**, 1180 (2003).
[8] S. Rios *et al.*, J. Phys. Condens. Matter **15**, L305 (2003).
[9] H.M. Christen *et al.*, Appl. Phys. Lett. **68**, 1488 (1996).
[10] J. Sigman *et al.*, Phys. Rev. Lett. **88**, 097601 (2002).
[11] M. Sepliarsky, S.R. Phillpot, and D. Wolf, J. Appl. Phys. **90**, 4509 (2001).
[12] M. Sepliarsky *et al.*, J. Appl. Phys. **91**, 3165 (2002).
[13] J.C. Jiang *et al.*, Appl. Phys. Lett. **74**, 2851 (1999).
[14] F. Le Marrec *et al.*, Phys. Rev. B **61**, R6447 (2000).
[15] C. Bungaro and K.M. Rabe, Phys. Rev. B **65**, 224106 (2002); Phys. Rev. B **69**, 184101 (2004).
[16] H.N. Lee *et al.*, Nature (London) **433**, 395 (2005).
[17] I.P. Batra and B.D. Silverman, Solid State Commun. **11**, 291 (1972).
[18] J. Junquera and P. Ghosez, Nature (London) **422**, 506 (2003).
[19] M. Dawber, P. Chandra, P.B. Littlewood, and J.F. Scott, J. Phys. Condens. Matter **15**, L393 (2003).
[20] C. Lichtensteiger, J.-M. Triscone, J. Junquera, and P. Ghosez, Phys. Rev. Lett. **94**, 047603 (2005).
[21] D.D. Fong *et al.*, Science **304**, 1650 (2004).
[22] V. Nagarajan *et al.* (unpublished).
[23] *Landolt-Börnstetin, III, 16a*, edited by. K.H. Hellwege and A.M. Hellwege (Springer-Verlag, Berlin, 1981).
[24] R. Cohen, Nature (London) **358**, 136 (1992).
[25] This procedure is also valid in the case where the superlattice periodicity is not a whole number of unit cells and the x-ray peak positions are defined by the “real” superlattice wavelength (which can be much larger than the desired “pseudo” wavelength), though a small degree of error can arise in some cases. Errors can also arise due to interactions between the substrate peak and sample peaks as discussed by P.F. Fewster, Semicond. Sci. Technol. **8**, 1915 (1993). On the basis of kinematical theory simulations and x-ray measurements on samples with variable total thickness we found that for the $2n$th reflection used here to obtain $\bar{c}$ the errors from the first effect are always less than ±0.002 Å, and from the second effect less than ±0.003 Å, leading to our total error estimate of ±0.005 Å.
[26] P. Paruch, T. Tybell, and J.-M. Triscone, Appl. Phys. Lett. **79**, 530 (2001).
[27] X. Gonze *et al.*, Comput. Mater. Sci. **25**, 478 (2002).
[28] M. Teter, Phys. Rev. B **48**, 5031 (1993).
[29] The calculations provide $U(P_0) = BP_0^2 + CP_0^4$ and $c/a = \alpha + \beta P_0^2 + \gamma P_0^4$. For U in [eV/cell] and P_0 in [C/m^2]: $B_s = 0.210\,463\,31$, $B_p = -0.171\,752\,79$, $C_s = 0.309\,134\,20$, $C_p = +0.160\,684\,41$, $\alpha_s = 1.0$, $\alpha_p = 1.015\,661\,46$, $\beta_s = 0.060\,769\,52$, $\beta_p = 0.036\,099\,15$, $\gamma_s = 0.048\,203\,68$, $\gamma_p = 0.022\,090\,09$.
[30] Na Sai, K.M. Rabe, and D. Vanderbilt, Phys. Rev. B **66**, 104108 (2002).
[31] G. Kresse and J. Furthmüller, Phys. Rev. B **54**, 11 169 (1996).
[32] P.E. Blöchl, Phys. Rev. B **50**, 17 953 (1994).
[33] G. Kresse and D. Joubert, Phys. Rev. B **59**, 1758 (1999).
[34] The ABINIT [27] and VASP calculations have been done with different pseudopotentials, cutoffs, and exchange-correlation functionals, which collectively account for the difference in the c axis lattice parameter obtained for $PbTiO_3$. For this reason, we compare fractional changes in the structural parameters, rather than absolute values, as n_s and n_p vary.
[35] R.D. King-Smith and D. Vanderbilt, Phys. Rev. B **47**, R1651 (1993).
[36] S. Tinte, K.M. Rabe, and D. Vanderbilt, Phys. Rev. B **68**, 144105 (2003).